Direct visualization of the periodic displacement of Ta atoms in the commensurate charge density wave phase of $1T$-TaSe$_2$ in real space

Keita Kobayashi[1,*] and Hidehiro Yasuda[1,2,†]

[1]*Research Center for Ultra-High Voltage Electron Microscopy, Osaka University, 7-1, Mihogaoka, Ibaraki, Osaka 567-0047, Japan*

[2]*Division of Materials and Manufacturing Science, Graduate School of Engineering, Osaka University, 2-1,*
Yamadaoka, Suita, Osaka 565-0871, Japan

In $1T$-TaSe$_2$, annular dark-field scanning transmission electron microscopy (ADF-STEM) of the commensurate charge density wave (CCDW) phase shows the periodic image contrast superimposed on the atomic columns. The periodicity of the image contrast is consistent with the superlattice formed by the periodic displacement of Ta atoms by the CCDW. Comparing the ADF-STEM with simulated images shows that the image contrast is formed by the displacement of Ta atoms. This result means that the displacement of Ta atoms by the CCDW is directly observed in real space and suggests that a coherent CDW forms on every layer of $1T$-TaSe$_2$.

Some transition metal dichalcogenides (TMDCs) form a charge density wave (CDW) on their two-dimensional atomic layered structure and electronic system due to Peierls instability [1–3]. In the CDW phase, the positions of transition metal atoms in TMDCs are displaced periodically, and a supercell is formed. To understand the changes in the structure and physical properties of TMDCs due to CDWs and their mechanisms, it is desirable to visualize the geometrical fluctuations of the transition metal atom positions in real space. To date, the formation of supercells has been shown in real space by transmission electron microscopy (TEM) [4–8] and scanning tunneling microscopy (STM) [9–11]. However, because the supercell in TEM images is imaged by phase contrast, the details of the geometrical fluctuations of the transition metal atom positions are not visible. STM images of the CDW phase of TMDCs also show periodic image contrast fluctuation consistent with the periodicity of the supercell. However, the fluctuation of the image contrast in the STM images reflects the charge modulation on the surface of TMDCs [11] and does not show the transition metal atom positions. Moreover, because chalcogen atoms are located on the outermost surface of TMDCs, the STM image does not reflect the positions of transition metal atoms directly [11]. Therefore, although the model of the transition metal atom displacement in the CDW phase transition was proposed by electron diffractometry in 1974 [2], it has not been confirmed experimentally by direct observation in real space. Hence, visualizing the displacement in real space remains a challenge and is important to solid physics.

In contrast to TEM and STM, the image contrast in annular dark-field scanning TEM (ADF-STEM) is determined in relation to the atom positions in the specimen. Therefore, the morphology and fluctuation of the displacement of the transition metal atoms in the CDW phase of TMDCs can be interpreted intuitively from the ADF-STEM image. In this study, we visualized the displacement of transition metal atoms in the CDW phase of TMDCs in real space by ADF-STEM. We examined the structural fluctuations to provide evidence

for the model and to reveal the detailed structure of the CDW phase of TMDCs. We used $1T$-TaSe$_2$, which is a typical TMDC that shows a commensurate CDW (CCDW) phase at room temperature [2,3] (CCDW phase transition temperature: $T_{CCDW} = 473$ K; incommensurate CDW [ICDW] phase transition temperature: $T_{ICDW} = 600$ K [12]). We observed additional periodic image contrast, which is consistent with the periodicity of the supercell of the CCDW phase of $1T$-TaSe$_2$, superimposed on image contrasts arising from atomic columns. We report the morphology of the image contrast and discuss the imaging mechanism of the contrast in comparison with simulated ADF-STEM images. Then, we describe the displacement of Ta atom positions in the CCDW phase of $1T$-TaSe$_2$ and the coherent CDW formation on every layer of $1T$-TaSe$_2$ revealed by the observations.

$1T$-TaSe$_2$ single crystals for the specimen were prepared by the chemical vapor transport method [13–16]. The obtained single crystals were cleaved perpendicular to the c-axis. The structures of the specimens were confirmed by conventional TEM (Hitachi, H-800 or H-800B). ADF-STEM images were observed using an atomic-resolution analytical TEM (JEOL, JEM-ARM200F/UHR). The image simulation was performed with the multislice method (HREM, xHREM ver. 3.6.0.5.1) [17]. Detailed specimen preparation and the experimental method are shown in the Supplemental Material [18].

Figure 1(a) shows a typical transmission electron diffraction (TED) pattern of a $1T$-TaSe$_2$ single crystal acquired from the c-axis at 296 K (corresponding TEM image is shown in the Supplemental Material [18]). In the TED pattern, there are many satellite reflections around the fundamental diffraction patterns, indicating the formation of a superlattice structure by the periodic displacement of Ta atoms in the $1T$-TaSe$_2$ by CDW [2,3]. In addition, the first-order long-period reflections [denoted by an arrow head in Fig. 1(a)], which are forbidden reflections in the TED pattern of the nearly CCDW (NCCDW) phase of $1T$-TaS$_2$ [6,8], are visible in the TED pattern. The disappearance of the reflection spots in the TED pattern of the NCCDW phase of $1T$-TaS$_2$ can be attributed to the formation of a CDW with a threefold periodic structure along the c-axis [6,8]. Therefore, our TED patterns may show that a coherent CDW is formed in every layer of the CCDW phase of $1T$-TaSe$_2$. Figure 1(b) shows a TED pattern of the same region

*kobayashi-z@uhvem.osaka-u.ac.jp
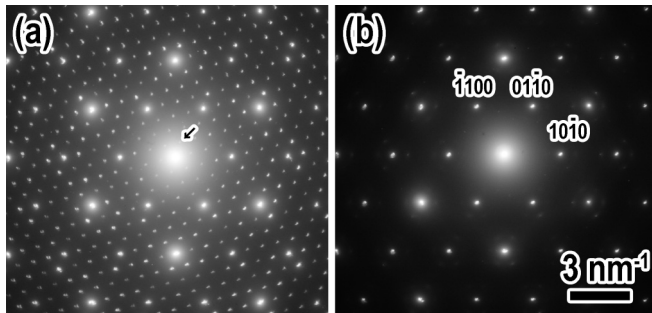†yasuda@uhvem.osaka-u.ac.jp

FIG. 1. Typical TED pattern of $1T$-TaSe$_2$ acquired at (a) 296 and (b) 673 K.

for the specimen at 673 K, which is above the phase transition temperature from the ICDW phase to the normal phase of $1T$-TaSe$_2$ [12]. In contrast to the TED pattern acquired at 296 K, no satellite reflections are observed in the TED pattern because the Ta atom positions in $1T$-TaSe$_2$ are ordered by the phase transition to the normal phase.

Figures 2(a) and 2(b) respectively show high- and low-magnification ADF-STEM images of $1T$-TaSe$_2$ acquired from the c-axis at 296 K. The Ta and Se atomic columns, which correspond to spots with strong and weak contrast, respectively, are resolved clearly in the high-magnification image. In the low-magnification image, a periodic image contrast with sixfold symmetry is seen in addition to the atomic columns. Figure 2(b) also shows the fast Fourier transform (FFT) pattern corresponding to the low-magnification image. The FFT pattern shows many additional spots that are consistent with the superlattice reflection in the TED pattern of the CCDW phase of $1T$-TaSe$_2$ [Fig. 1(a)], in addition to the patterns that correspond to the fundamental lattice diffraction. Because the superimposed rotation diffraction patterns are not observed in the FFT and TED patterns obtained from the same region in the specimen, and the STEM probe size for the low-magnification ADF-STEM images is small enough to resolve the lattice distances of $1T$-TaSe$_2$, the periodic image contrast is not caused by rotation moiré [19] and a scanning moiré fringe [20]. Figure 2(c) shows the ADF-STEM image and corresponding FFT pattern of $1T$-TaSe$_2$ acquired at 673 K. In contrast to Fig. 2(b), no periodic image contrast except for the atomic columns is observed in the ADF-STEM image. Furthermore, the corresponding FFT pattern shows only the patterns that correspond to the fundamental lattice diffraction. This result is consistent with the change in the TED pattern owing to the phase transition caused by heating shown in Fig. 1(b). The result shows that the periodic image contrast in the ADF-STEM image obtained at 296 K can be attributed to the periodic displacement of Ta atoms in the CCDW phase of $1T$-TaSe$_2$ (also refer to the Supplemental Material [18]).

To clarify the image interpretation and imaging mechanism of the periodic image contrast in the ADF-STEM image, we compared the image with simulated ADF-STEM images. In the model [2,3], Ta atoms in the CCDW phase of $1T$-TaSe$_2$ are considered to form clusters with hexagram morphology consisting of 13 Ta atoms because of periodic displacement of the atomic positions [Fig. 3(a)]. Consequently, the superlattice of the CCDW phase of $1T$-TaSe$_2$ corresponds to $\sqrt{13}a \times \sqrt{13}a \times c$, where a and c are the lattice
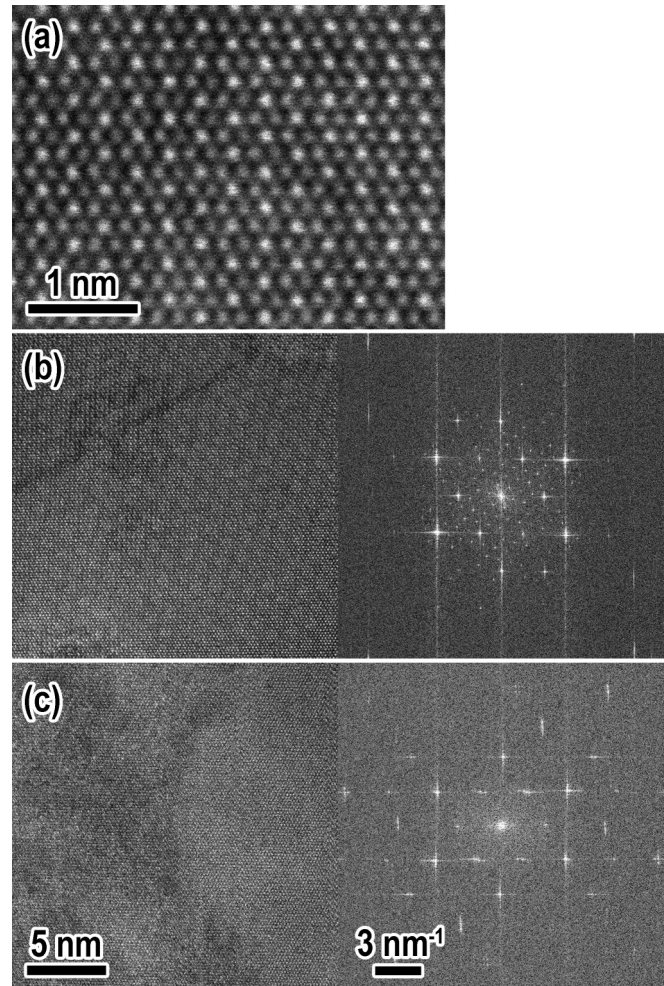

FIG. 2. (a) High-magnification ADF-STEM image of $1T$-TaSe$_2$ acquired at 296 K. ADF-STEM image and corresponding FFT pattern of $1T$-TaSe$_2$ acquired at (b) 296 and (c) 673 K.

constants of the normal phase of $1T$-TaSe$_2$ ($a = 0.3478$ nm, $c = 0.6263$ nm), rotated by 13.9° relative to the a-axis of the normal phase of $1T$-TaSe$_2$ [3]. In the simulation, the model structure of the CCDW phase of $1T$-TaSe$_2$ is a crystal with a unit cell consistent with the superlattice. The coordinates and Debye-Waller factors of all atoms in the unit cell (shown in the Supplemental Material [18]), which are reflected in the displacement of the Ta atom positions in the CCDW phase and affect the displacement of the Se atom positions, are obtained by modifying the previous X-ray diffractometry data [21,22]. The data are for the octahedral layer in $4H_b$-TaSe$_2$ at room temperature, which shows the same CDW phase transition as $1T$-TaSe$_2$.

The Debye-Waller factors of Ta atoms fluctuate depending on their coordinates, whereas those of Se atoms in the cell are constant. Figure 3(b) shows the simulated ADF-STEM image of the CCDW phase of $1T$-TaSe$_2$. The sample thickness and defocus value are 62.6 and 48.3 nm (under focus), respectively. The simulated image shows a periodic image contrast that is consistent with the periodicity of the periodic image contrast in the ADF-STEM image of the CCDW phase of $1T$-TaSe$_2$.
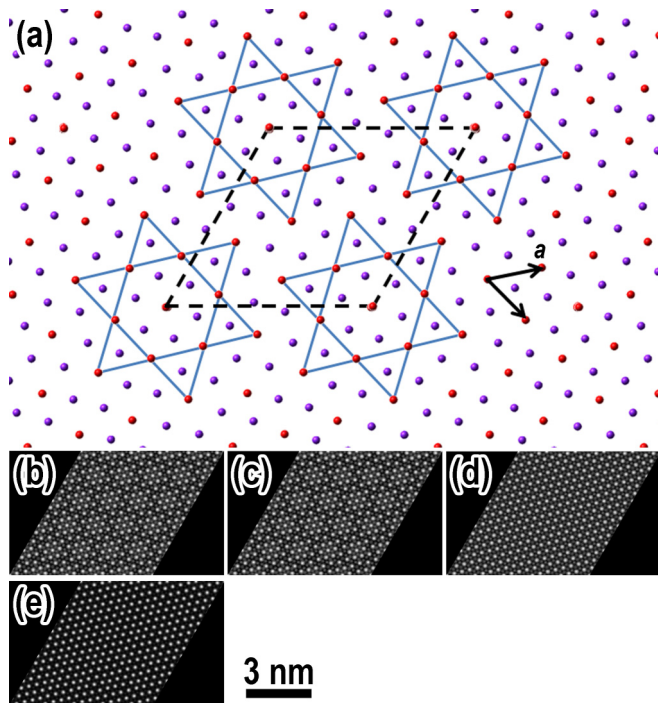
FIG. 3. (a) Schematic representation of the periodic displacement of Ta atom positions in the CCDW phase of $1T$-$TaSe_2$. Red circles and purple circles indicate Ta and Se atoms, respectively. The Ta atom positions are displaced periodically to form clusters with hexagram morphology consisting of 13 Ta atoms. The cell indicated by dashed lines shows the superlattice of the CCDW phase of $1T$-$TaSe_2$. Black arrows show the translation vectors of the unit cell of the normal phase of $1T$-$TaSe_2$. (b) Simulated ADF-STEM images of the CCDW phase of $1T$-$TaSe_2$ using the model shown in (a). (c) The model with an averaged Debye-Waller factor for Ta atoms. (d) A model that does not reflect the displacement of Ta and Se atom positions in the CCDW phase. (e) A model that consists of three layers of the CCDW phase of $1T$-$TaSe_2$ with periodic deviation to form a deviated CDW in every layer.

FIG. 4. (a) ADF-STEM image of $1T$-$TaSe_2$ and corresponding FFT pattern. (b) Line profile of image contrast intensities of Ta atomic columns along x to x′ shown in (a). (c) Line profile of image contrast intensities of Ta and Se atomic columns along y to y′ shown in (a).

The ADF-STEM images are mainly formed from thermal diffuse scattering (TDS) electrons. The TDS scattering cross section of a specimen is a function of the Debye-Waller factor [23,24]; thus, the fluctuation of the Debye-Waller factor of Ta atoms depending on their coordinates may contribute to forming the periodic contrast. To clarify the contribution of the Debye-Waller factor difference, the simulation was also performed using a model structure with a homogeneous Debye-Waller factor for the Ta atoms. Figure 3(c) shows the simulated ADF-STEM image of $1T$-$TaSe_2$ formed under the same conditions as in Figure 3(b), except that the Debye-Waller factor is averaged as $9.10 \times 10^{-3} \ nm^2$. The simulation image shows similar periodic image contrast to Figure 3(b). The result suggests that the fluctuation of the Debye-Waller factor of Ta atoms does not contribute to the formation of the periodic image contrast in the ADF-STEM image as a dominant factor.

Figure 3(d) shows the simulated ADF-STEM image of $1T$-$TaSe_2$ formed by the model structure, which is not reflected in the displacement of the Ta and Se atom positions in the CCDW phase. Although the unit cell of the model is the
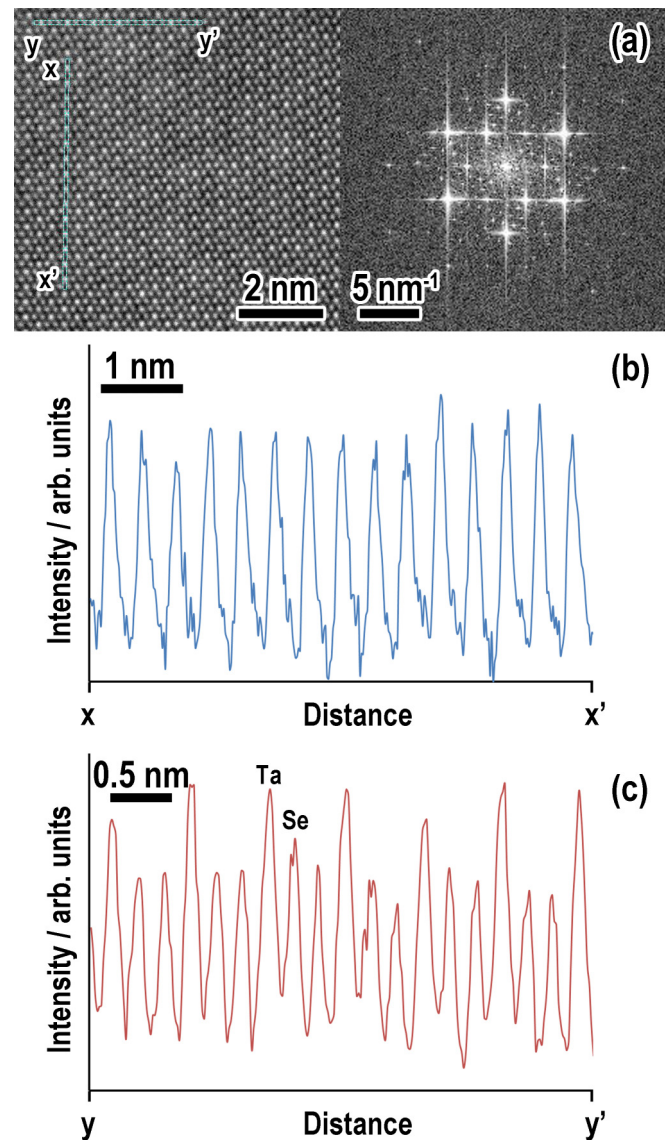
same as the superlattice of the CCDW phase of $1T$-$TaSe_2$, the coordinates of all the atoms in the unit cell are the same as the normal phase of $1T$-$TaSe_2$. The Debye-Waller factor of the Ta atoms is set to $9.10 \times 10^{-3} \ nm^2$. The simulated ADF-STEM image was formed under the same conditions as the previous simulations, except for the simulation model. In the simulated image, no periodic image contrast is observed, strongly suggesting that the periodic image contrast in the ADF-STEM image is formed by the displacement of Ta atoms.

This conclusion is supported by experimental observation of image contrast intensities in Ta atomic columns in the ADF-STEM image. Figure 4(a) shows the ADF-STEM image of the CCDW phase of $1T$-$TaSe_2$ acquired at 296 K and the corresponding FFT pattern. To increase the signal-to-noise ratio, the image was obtained by summing 50 ADF-STEM

images acquired in the same region with specimen-drift correction. The ADF-STEM image shows the periodic image contrast superimposed on the atomic columns. The satellite spots around the fundamental diffraction patterns shown in the corresponding FFT pattern also indicate the appearance of the periodic image contrast in the ADF-STEM image. Figure 4(b) shows the line profile of the image contrast intensities of 15 Ta atomic columns along x to x' in Fig. 4(a). The first Ta atomic column on the line profile is positioned at the center of the periodic image contrast. The Debye-Waller factors of Ta atoms on the line profile fluctuate periodically in the 13 Ta atom cycle (shown in the Supplemental Material [18]). However, the image contrast shows no periodicity in the line profile. Although fluctuation of the image contrast of Ta atomic columns is confirmed in the line profile, the intensities are different from those in the periodic image contrast. Figure 4(c) shows the line profile of the image contrast intensities of Ta and Se atomic columns along y to y'. The strong peaks are attributed to Ta atomic columns. The two weak peaks between the strong peaks are attributed to Se atomic columns. The variance of intensities of Ta atomic columns along x to x' is almost equivalent to that of the Se atomic columns. This result suggests that the contribution of the fluctuation in the Debye-Waller factor to the fluctuation of the image contrast of the Ta atomic columns is negligible.

In contrast to TEM and STM images, the ADF-STEM image shows the position of the atomic columns directly. Therefore, the periodic image contrast reflects the periodic density fluctuations of the Ta atomic columns formed by the static displacement of Ta atom positions, and thus the geometrical fluctuation of the Ta atom positions on the CCDW phase of $1T$-TaSe$_2$ in real space is directly visualized. Moreover, the Ta displacement model proposed in previous studies [2,3,21,22] is confirmed by the morphology and periodicity of the periodic image contrast shown in the ADF-STEM image.

The image simulations assume that the CDW forms homogeneously on every layer of $1T$-TaSe$_2$, and thus simulation models are formed by stacking the layers homogeneously. However, the NCCDW phase of $1T$-TaS$_2$ forms a CDW that alters its phase along the c-axis [6,8]. Because the displacement of the Ta atom position depends on the phase of the CDW, the amplitudes of the displacement of the Ta atom positions of the $1T$-TaS$_2$ are averaged along the c-axis. The incoherent CDW model is reasonable, because it decreases the electrostatic repulsion between each layer. Therefore, consideration of the ADF-STEM image contrast of the CCDW phase of $1T$-TaSe$_2$, if an incoherent CDW forms in the layers, is important to confirm the structure of the CCDW phase of $1T$-TaSe$_2$ and the imaging mechanism of the periodic image contrast. Figure 3(e) shows the simulated ADF-STEM

image of $1T$-TaSe$_2$. The model structure for this simulation consists of three monolayers of the CCDW phase of $1T$-TaSe$_2$ showing periodic deviation to form a deviated CDW in every layer. The simulated ADF-STEM image was formed under the same conditions as Fig. 3(b), except for the simulation model. The periodic image contrast is also not observed in the simulated image. As shown in the TED pattern of the CCDW phase of $1T$-TaSe$_2$ [Fig. 1(a)], the formation of a coherent CDW is implied. In addition to the experimental result, the similarity of the experimental ADF-STEM image and the simulated image from the coherent CDW model strongly suggests that the coherent CDW is formed in the CCDW phase of $1T$-TaSe$_2$.

In this study, in the ADF-STEM image of the CCDW phase of $1T$-TaSe$_2$, we demonstrated that a periodic image contrast with periodicity consistent with that of the superlattice appears in addition to the atomic column contrasts. By comparing the ADF-STEM image with the simulated image, we showed that the periodic image contrast reflects the periodic density fluctuation of the Ta atomic columns formed by the static displacement of the Ta atom positions. Therefore, we have directly visualized the geometrical fluctuation of Ta atom positions, which correspond to the model proposed in previous studies, in the CCDW phase of $1T$-TaSe$_2$ in real space. Moreover, the TED pattern of the CCDW phase of $1T$-TaSe$_2$ and the similarity of the experimental ADF-STEM image to the images simulated with the coherent CDW model suggest that the coherent CDW is formed in every layer of the CCDW phase of $1T$-TaSe$_2$.

An important result of this study is observation of the unknown fine structure of CDW directly in real space. We also discovered the defect structure of CDW on the CCDW phase of $1T$-TaSe$_2$ (shown in the Supplemental Material [18]) by direct observation, in addition to the periodic displacement of Ta atoms and the coherent CDW. These unknown fine structures may be the origin of the properties which cannot be expected from structures determined by theory and conventional macroscopic analyses. Different from the CCDW phase of $1T$-TaSe$_2$, some TMDCs (e.g., $1T$-TaS$_2$ [25,26]) show properties which cannot be expected from the band structures. Exploring the fine structures by direct observation in real space may clarify these unresolved issues. Although the actual physics of $1T$-TaSe$_2$ related to these fine structures remain unclear, the results and the technique presented here will contribute to further physics research of $1T$-TaSe$_2$ and will also be important to the development of solid physics of the CDW phase of low-dimensional materials.

[1] R. E. Peierls, *Quantum Theory of Solids* (Clarendon Press, Oxford, 1955), p. 108.

[2] J. A. Wilson, F. J. Di Salvo, and S. Mahajan, Phys. Rev. Lett. **32**, 882 (1974).

[3] J. A. Wilson, F. J. Di Salvo, and S. Mahajan, Adv. Phys. **24**, 117 (1975).

[4] J. van Landuyt, G. van Tendeloo, and S. Amelinckx, Phys. Status Solidi A **29**, K11 (1975).

[5] G. van Tendeloo, J. van Landuyt, and S. Amelinckx, Phys. Status Solidi A **64**, K105 (1981).

[6] M. Kuwabara, M. Yomita, H. Hashimoto, and H. Endoh, Phys. Status Solidi A **96**, 39 (1986).

[7] M. Kuwabara, H. Hashimoto, and H. Endoh, Jpn. J. Appl. Phys. **25**, L1 (1986).

[8] M. Kuwabara, Ph.D. dissertation, Osaka University, 1986.

[9] W. Han, E. R. Hunt, O. Pankratov, and R. F. Frindt, Phys. Rev. B **50**, 14746 (1994).

[10] J.-J. Kim, W. Yamaguchi, T. Hasegawa, and K. Kitazawa, Synth. Met. **70**, 1271 (1995).

[11] A. Kikuchi and M. Tsukada, Surf. Sci. **326**, 195 (1995).

[12] F. J. Di Salvo, J. A. Wilson, B. G. Bagley, and J. V. Waszczak, Phys. Rev. B **12**, 2220 (1975).

[13] F. Lévy, Nuovo Cim. **38**, 359 (1977).

[14] H. Yasuda and H. Fujita, J. Jpn. Inst. Metals **53**, 1191 (1989).

[15] R. Huisman and F. Jellinek, J. Less-Common Metals **17**, 111 (1969).

[16] R. Brouwer and F. Jellinek, Physica B **99**, 51 (1980).

[17] K. Ishizuka, Ultramicroscopy **90**, 71 (2002).

[18] See Supplemental Material at http://link.aps.org/supplemental/10.1103/PhysRevB.94.201409 for additional data.

[19] J. H. Warner, M. H. Rümmeli, T. Gemming, B. Büchner, and G. A. D. Briggs, Nano Lett. **9**, 102 (2009).

[20] D. Su and Y. Zhu, Ultramicroscopy **110**, 229 (2010).

[21] R. Moret and E. Tronc, Philos. Mag. B **40**, 305 (1979).

[22] J. Lüdecke, S. van Smaalen, A. Spijkerman, J. L. de Boer, and G. A. Wiegers, Phys. Rev. B **59**, 6063 (1999).

[23] S. J. Pennycook and D. E. Jesson, Ultramicroscopy **37**, 14 (1991).

[24] E. Abe, S. J. Pennycook, and A. P. Tsal, Nature (London) **421**, 347 (2003).

[25] J.-J. Kim, W. Yamaguchi, T. Hasegawa, and K. Kitazawa, Phys. Rev. Lett. **73**, 2103 (1994).

[26] O. Shiino, T. Endo, W. Yamaguchi, H. Sugawara, T. Hasegawa, and K. Kitazawa, Czech. J. Phys. **46**, 2621 (1996).